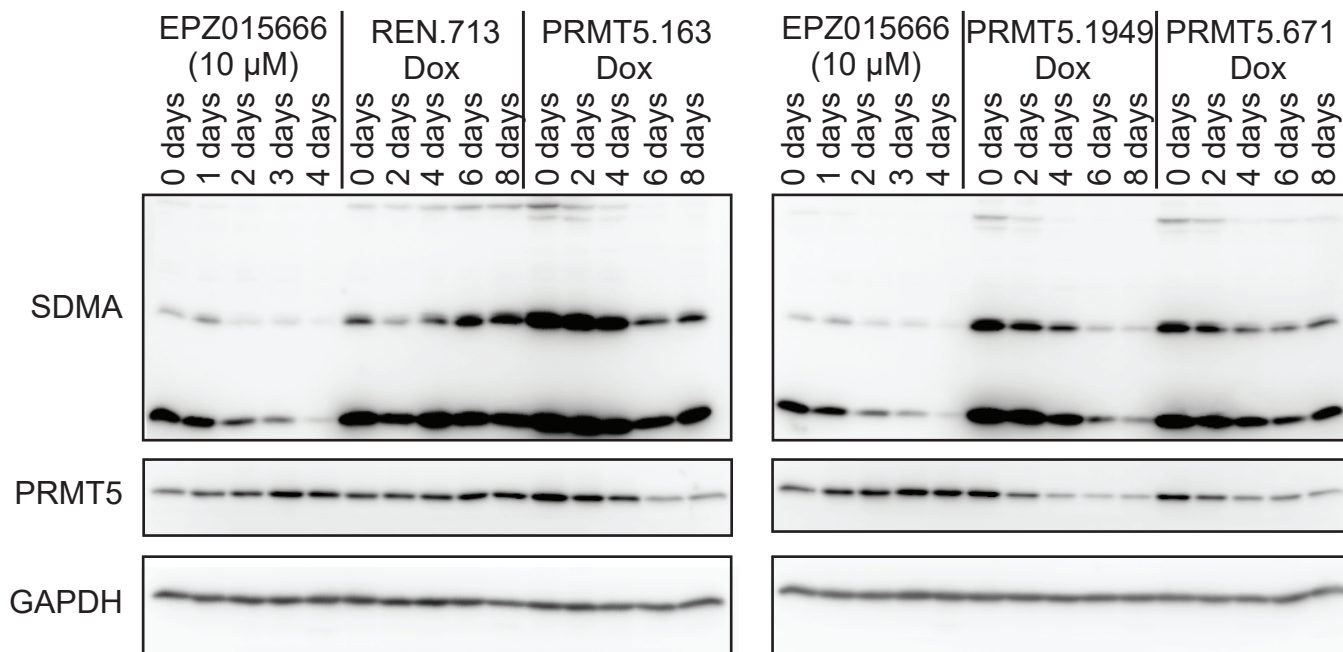
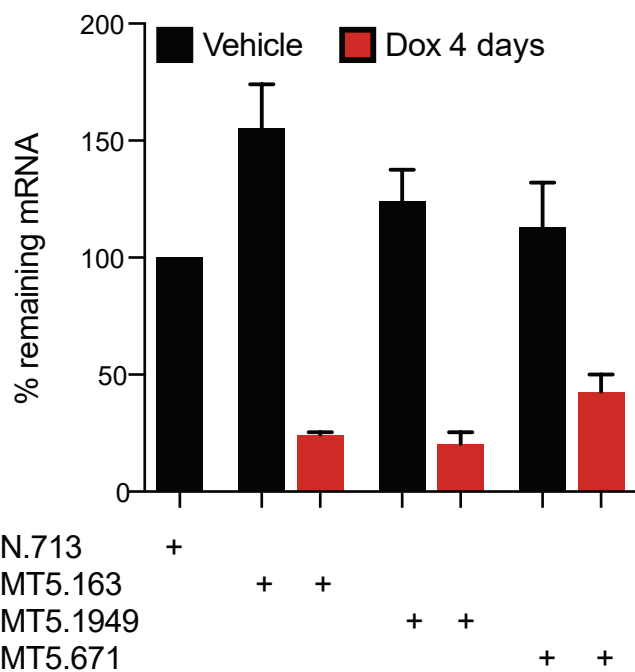
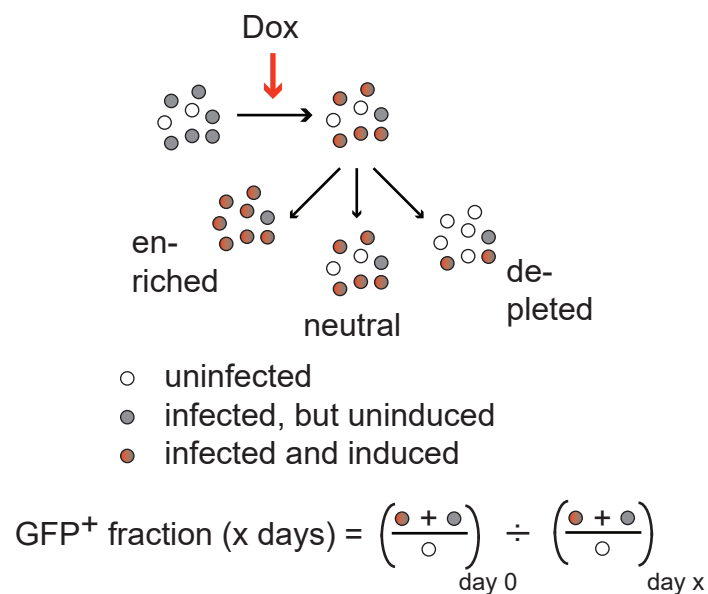
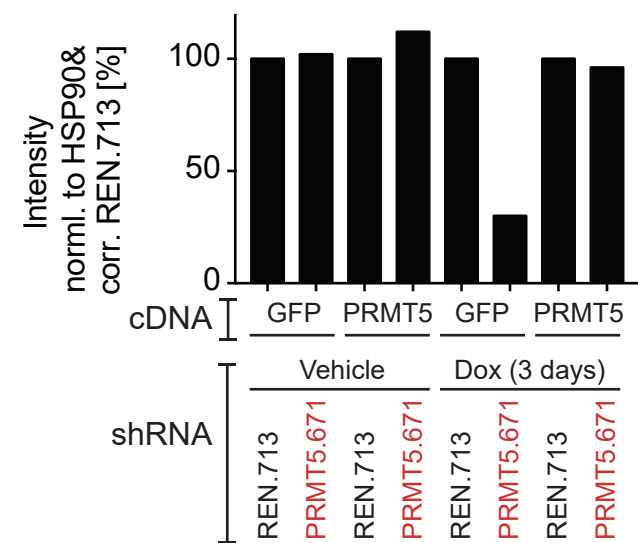
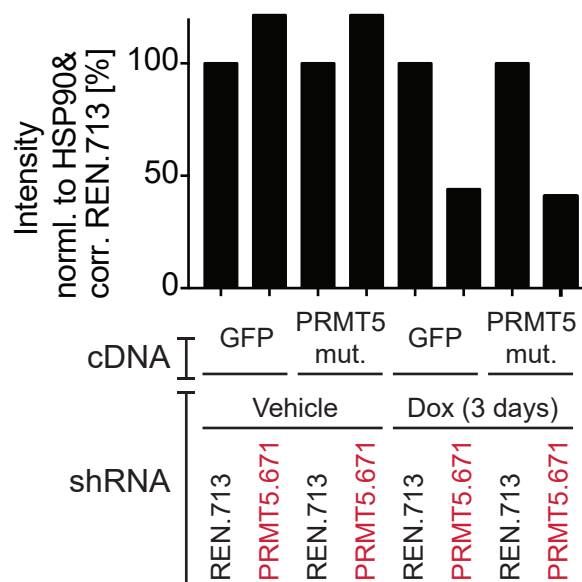


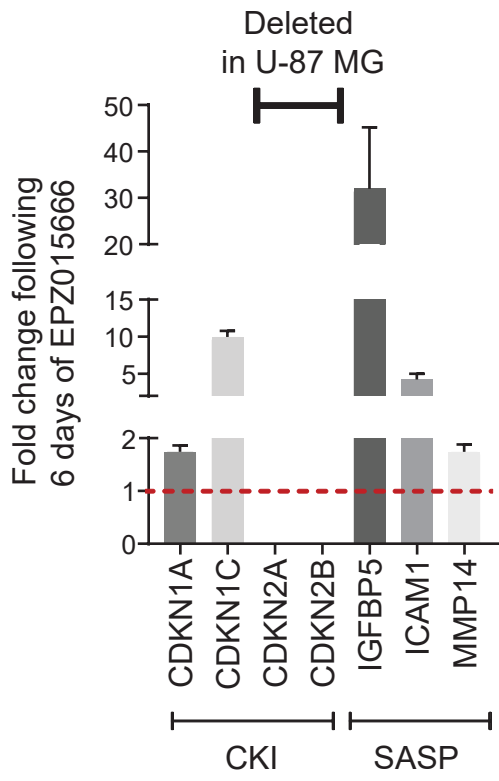
**Figure S1 (related to Figure 1). G1261 orthotopic *in vivo* model allows for precise dissection of tumor phenotypes and for high-coverage pooled transcriptome perturbation screens**

(A) qRT-PCR of KRAS mRNA levels in G1261 cells containing one of two KRAS targeting shRNAs, before and after doxycycline induction for 48 hr. n=3. Error bars represent +/- SEM. (B) *In vitro* competition assay, showing proportion of KRAS shRNA expressing cells compared to all shRNA transduced cells. n = 3. Error bars represent +/- SEM. (C) Immunoblot of G1261 cells probed for MGMT before and after retroviral MGMT cDNA overexpression. (D) Dot plot of *in vitro* competition assay using mixed populations of cells, a proportion of which are transduced with an MGMT overexpression vector that is also GFP<sup>+</sup>. Doses of TMZ represent a range of IC70-IC90, and cells were analyzed by flow cytometry after 96 hr. Left graph shows percent of GFP<sup>+</sup> cells, right graph shows fluorescence counts. n=3, lines represent mean +/- SD. (E) Scheme outlining GFP dilution assay performed by intracranial injection of a mixed population of G1261 cells containing a set percentage of cells expressing a retroviral GFP construct into C57BL6/J mice. The proportion of GFP<sup>+</sup> cells was determined in the final tumors by flow cytometry. (F) In GFP dilution assays, the percentage of GFP<sup>+</sup> cells acts as a surrogate for a certain library size (with lower GFP percentages representing larger libraries). The relationship between the percentage of GFP<sup>+</sup> cells in a mixed population and the modeled library size is: Library size = 1 / GFP%. (G) Plot showing correlation between different Illumina HiSeq lanes. Genomic DNA was isolated at t=0 from the same population of cells, but samples were PCR amplified separately and sequenced on different lanes. (H) Percentage of the library shRNAs present in the input (t=0), *in vitro*, and *in vivo* samples, with stringency > 0 or more reads (black bars) or >= 5 reads (grey bars). M = *in vivo* mouse samples, I = Tissue culture input controls, T = *in vitro* tissue culture samples. (I, J) Waterfall plots of all shRNAs across *in vitro* (I) and *in vivo* (J) samples depicting log fold change (logFC) of all shRNAs (grey), shRNAs targeting PRMT5 (red) and shRNAs targeting KRAS (blue) in comparison to t=0. (K,L) Dot plots depicting logFC of all shRNAs (grey), shRNAs targeting PRMT5 (red) and shRNAs targeting KRAS (blue) *in vitro* (K) and *in vivo* (L) in comparison to t=0. (M,N) Waterfall plots of all shRNAs across *in vitro* (M) and *in vivo* (N) samples comparing shRNAs enriched or depleted in response to TMZ versus respective vehicle treated control groups. (O) Hit identification pipeline across all four shRNA sub screens (*in vitro* – growth, *in vitro* – TMZ, *in vivo* – growth, *in vivo* – TMZ).

**A****B****C****D****E**

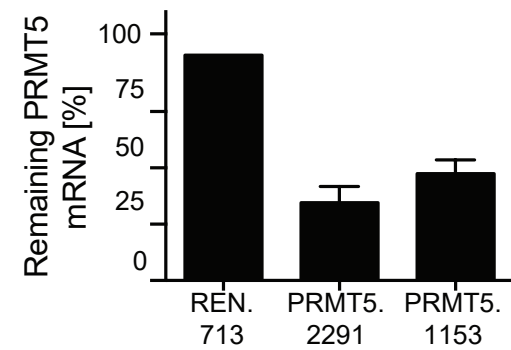
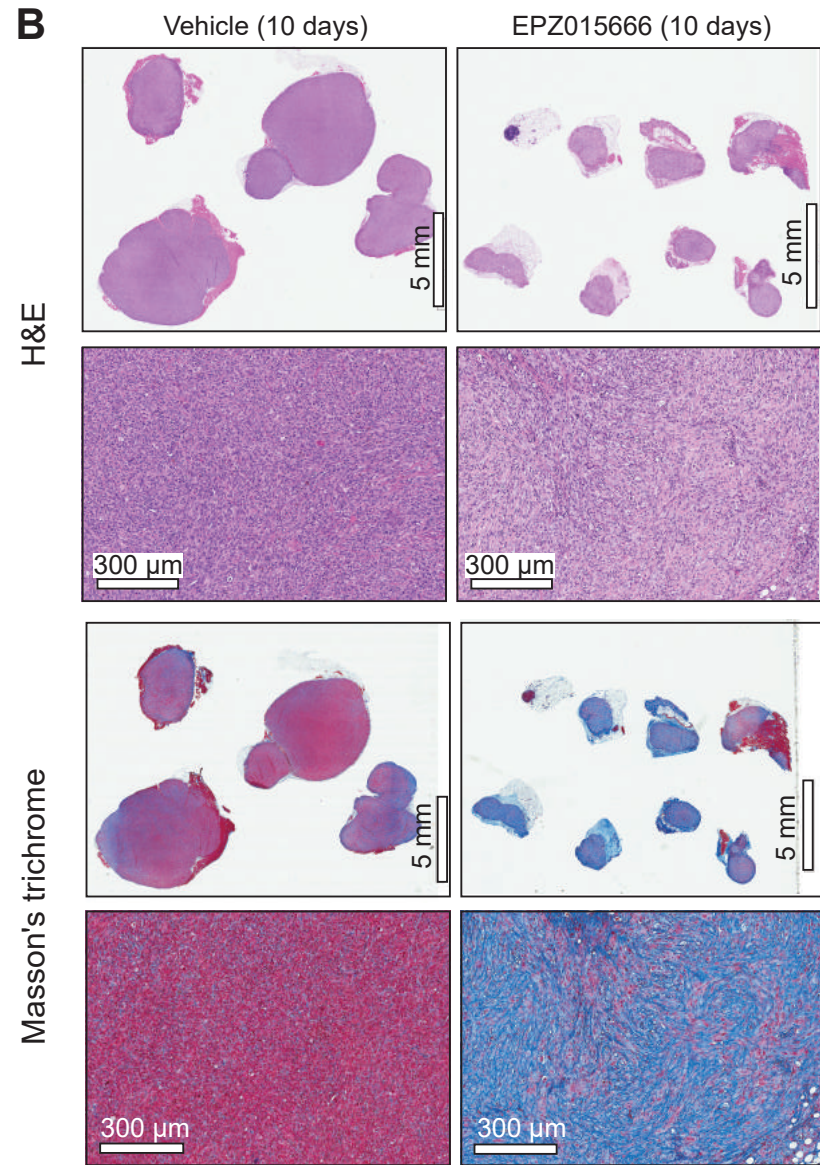
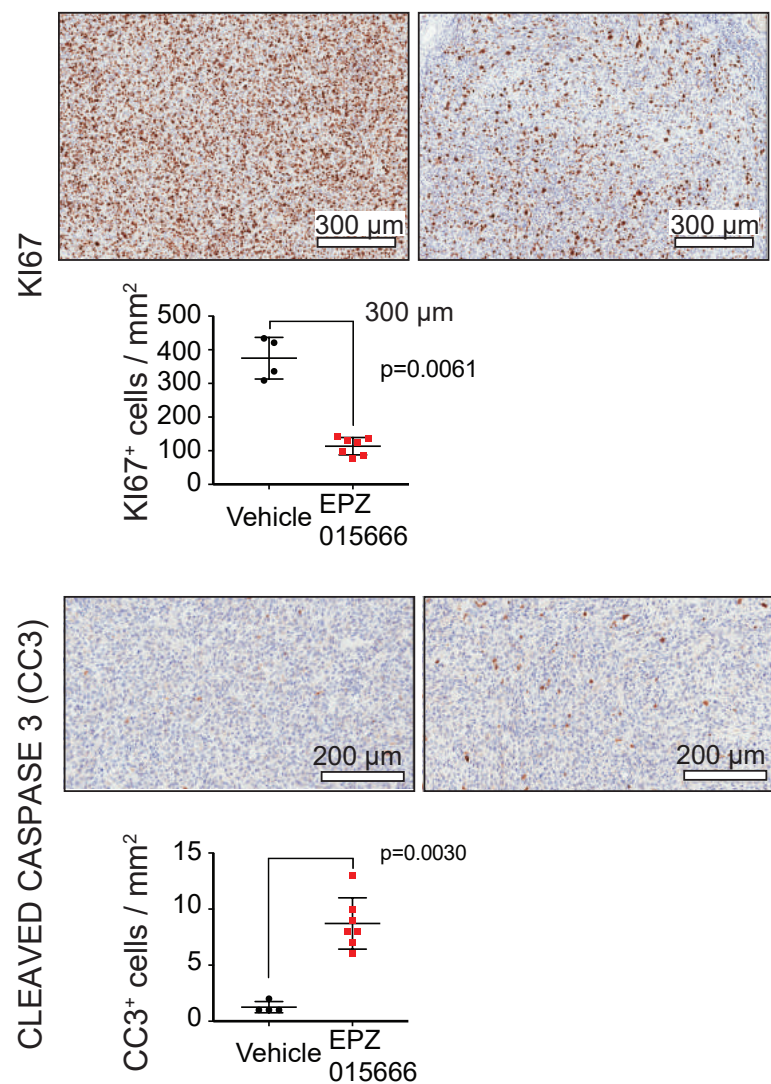
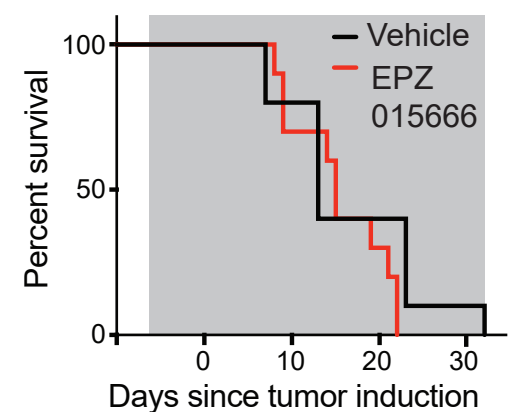
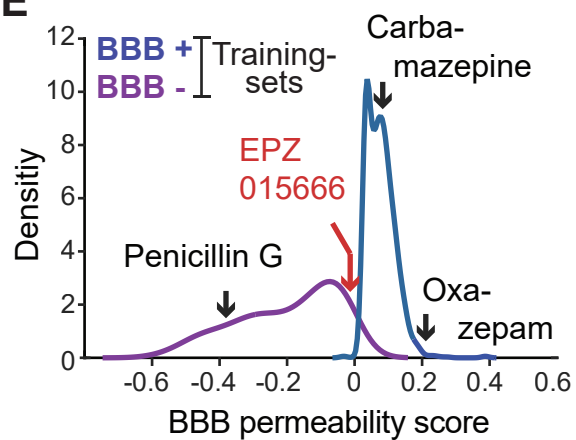
**Figure S2 (related to Figure 2). PRMT5 shRNAs inhibit PRMT5 function by causing a loss of PRMT5 mRNA and protein expression.**

(A) Immunoblot of U-87 MG cells treated either with 10  $\mu$ M EPZ015666 over a period of 4 days or induced for shRNA-mediated knockdown of PRMT5 using doxycycline over 8 days. (B) qRT-PCR of PRMT5 knockdown in U-87 MG cells with three different inducible shRNAs or a Renilla control shRNA. n=3, error bars depict +/- SD. (C) Scheme outlining competition assay: starting with a mixed population of cells where approximately half contain the shRNA vector and express Venus, addition of doxycycline induces expression of shRNA and dsRed. Over time, shRNA expressing cells are either enriched, depleted, or undergo no change with respect to the starting population, depending on the identity of the shRNA. (D) Immunoblot quantifications of Fig. 2E. Expression levels of H4R3me2s following PRMT5 knockdown were normalized to both HSP90 and REN.713 controls. (E) Immunoblot quantifications of Fig. 2H. Expression levels of H4R3me2s following PRMT5 knockdown were normalized to both HSP90 and REN.713 controls.

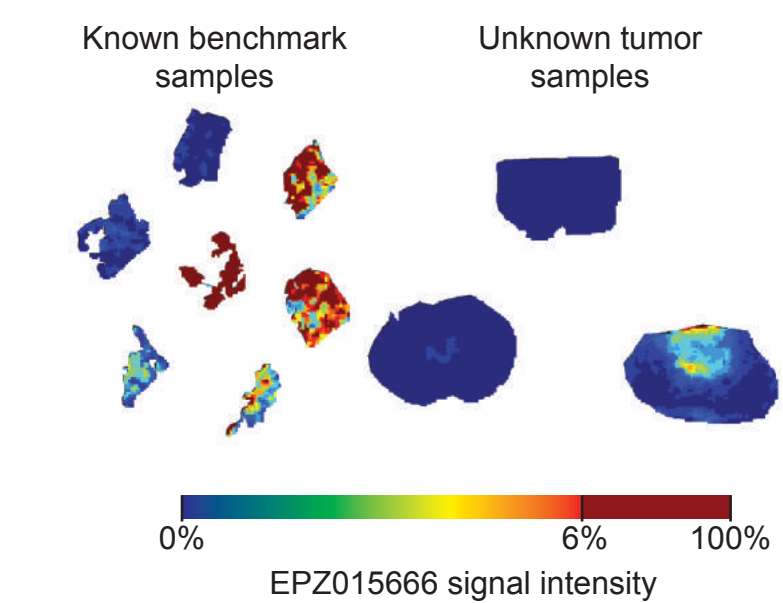
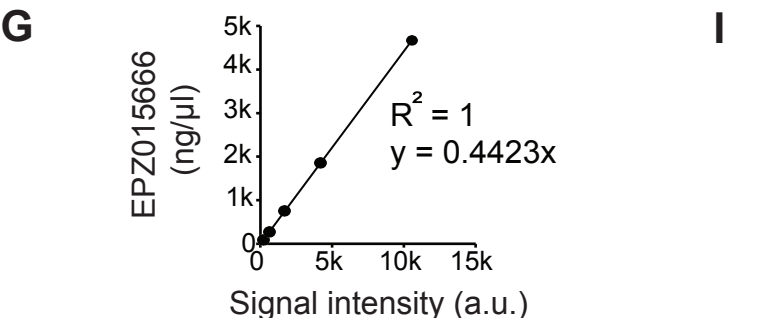
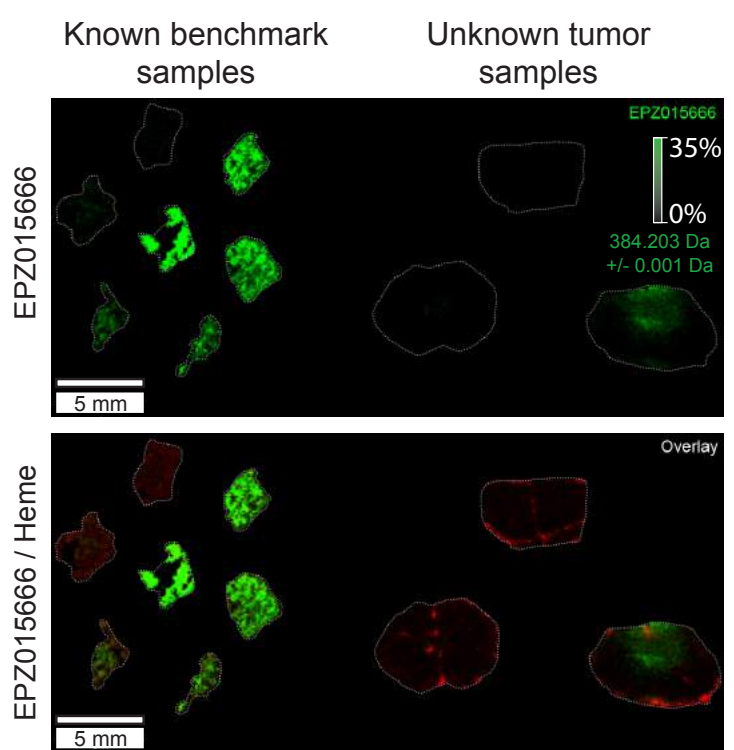
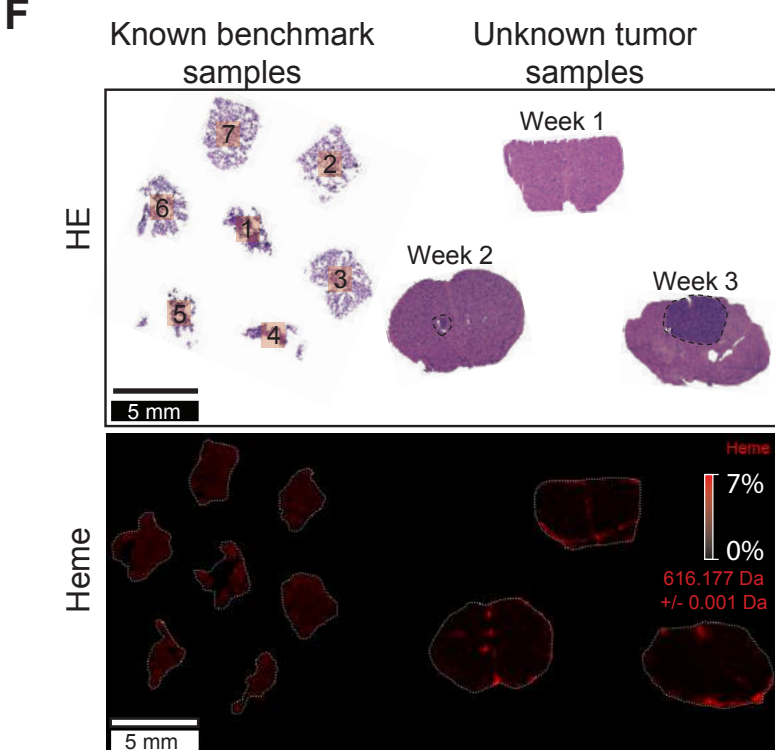


**Figure S3 (related to Figure 3). Tumor cells show increased expression levels of senescence associated transcripts following EPZ015666 treatment**

U-87 MG cells were treated with 10  $\mu$ M EPZ015666 / vehicle for 96 hr followed by RNA extraction, reverse transcription and qRT-PCR. Expression levels following EPZ015666 were normalized to GAPDH as an internal control and the corresponding expression level of vehicle treated cells. n=3, error bars represent +/- SEM. CKI = Cyclin-dependent kinase inhibitor proteins. SASP = Senescence-Associated Secretory Phenotype.

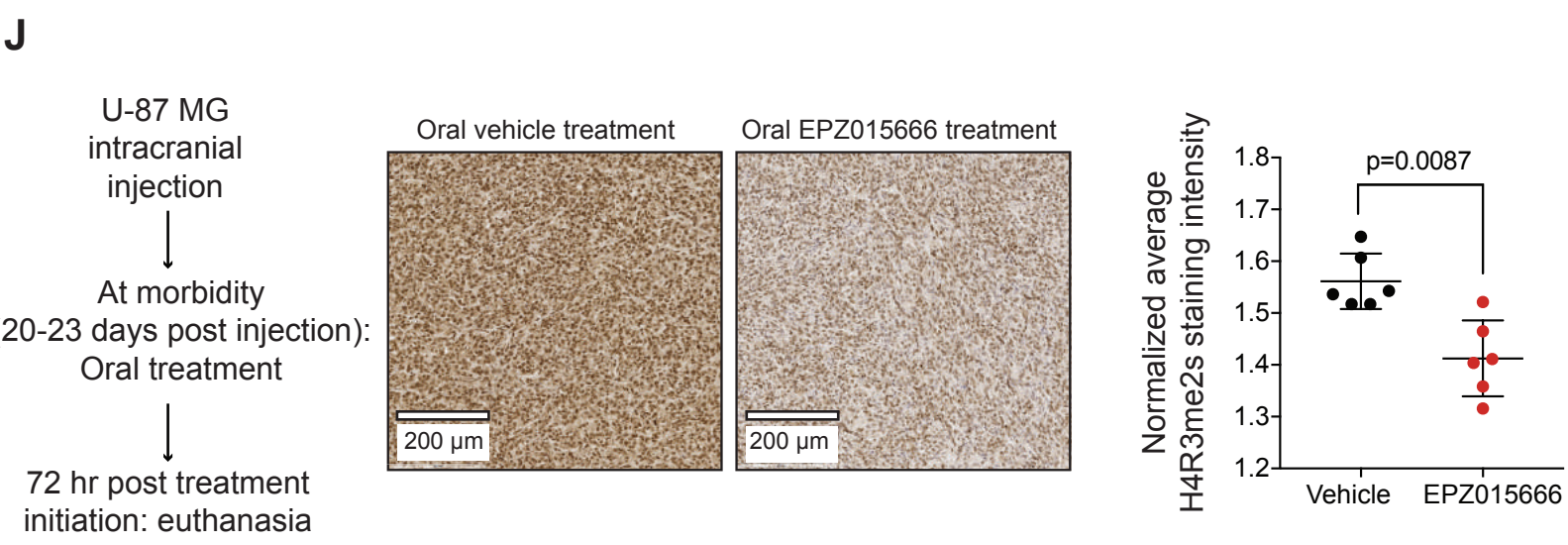
**A****B****C****D****E**



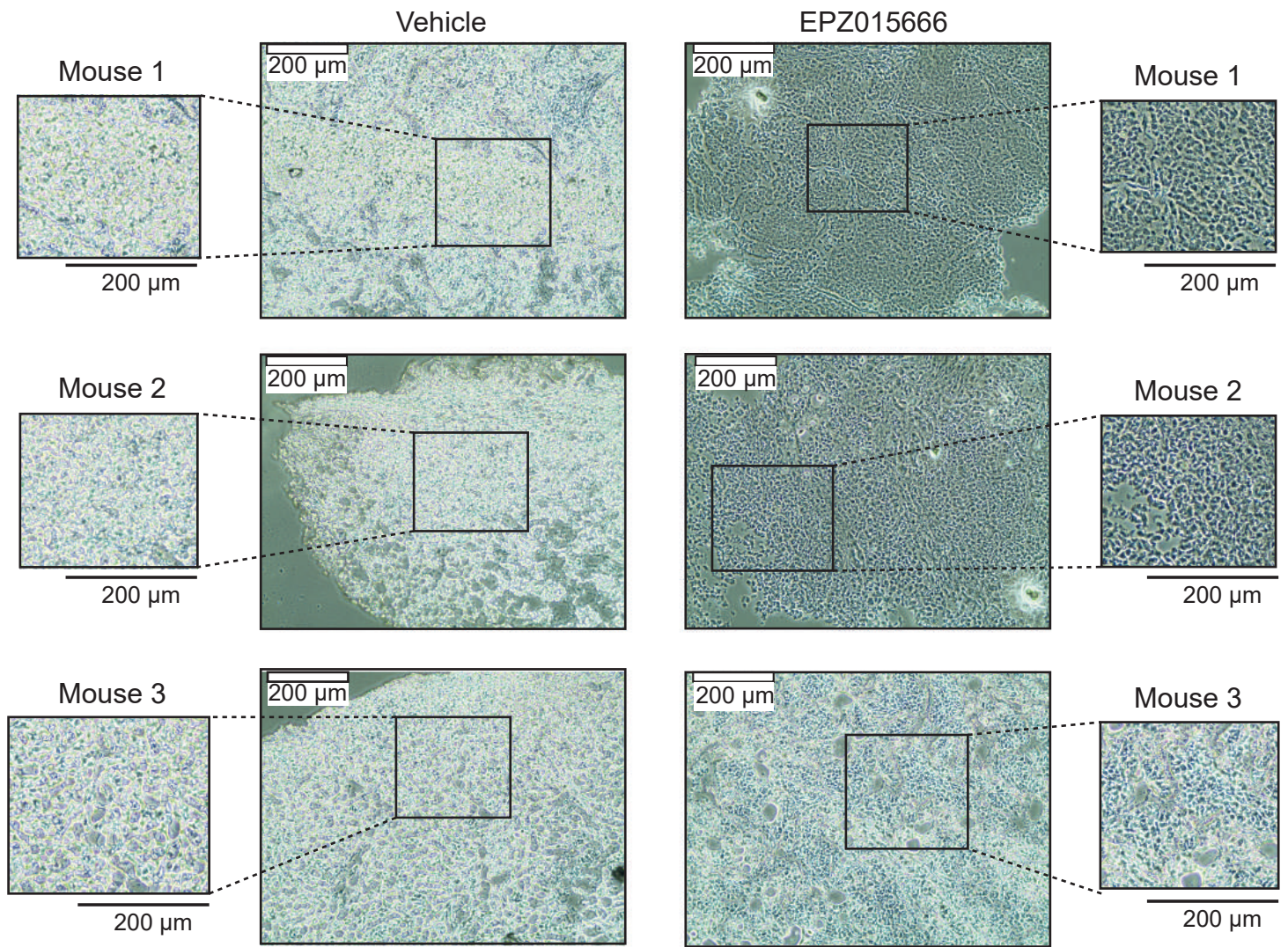


**H**

	Signal intensity (a.u.)	EPZ015666 (ng/g)
Week 1	216.63	95.813
Week 2 (all)	602.83	266.63
Week 2 (tumor only)	1695.74	750.03
Week 3 (all)	4198.28	1856.9
Week 3 (tumor only)	10557.70	4669.7





**K**

**Figure S4 (related to Figure 4). Despite being a poor penetrator of the blood brain barrier, EPZ015666 reaches advanced brain tumors due to leaky tumor vasculature**

(A) qRT-PCR showing shRNA mediated knockdown of PRMT5 by two constitutive PRMT5 shRNAs and one control shRNA targeting Renilla luciferase in GI261 cells. n=3, error bars represent +/- SEM. (B) H&E and Masson's trichrome staining of vehicle and EPZ015666 treated U-87 MG subcutaneous tumors. (C) KI67 or CC3 stains of subcutaneous U-87 MG tumors following EPZ015666 or vehicle treatment. Numbers of KI67<sup>+</sup> or CC3<sup>+</sup> cells were estimated in a blinded fashion and normalized to the counted areas. Bars represent mean and +/- SD. P values were calculated using Mann Whitney test. (D) Survival plot of C57BL/6J mice intracranially transplanted with GI261 cells and treated with vehicle or EPZ015666 (100 mg/kg, twice per day, treatment period highlighted in grey) starting on day 6 and continuing until the mice were euthanized due to high tumor burden. n=10 for each group. (E) *In silico* assessment of blood brain barrier permeability of EPZ015666 compared to other compounds. (F) Tissue mimetic models ("known benchmark samples") and brains from mice 1, 2 and 3 weeks after tumor injection were subjected to MALDI-MSI. (G) Normalization regression of MALDI-MSI signal intensity and known EPZ015666 concentration of tissue mimetic models. (H) Calculation of EPZ015666 concentration in unknown samples. Signal intensity (a.u.) was determined by MALDI-MSI and EPZ015666 concentration (ng/g) was then calculated based on normalization regression of tissue mimetic models. (I) Pseudo-colored pictures demonstrating EPZ015666 signal intensity of both known benchmark-samples and unknown tumor samples. (J) U-87 MG tumor cells were transplanted intracranially into the brains of nude mice and treated with EPZ015666 or vehicle for 72 hr. Tumors were sectioned and stained for H4R3me2s. Depicted is the normalized average of H4R3me2s staining intensity. Bars represent mean and +/- SD. Mann Whitney test used for significance testing. (K) MGG8 PDX glioma tumor cells were transplanted subcutaneously and treated with EPZ015666 or vehicle starting at day 9 post tumor implantation. Upon euthanasia, tumors were flash frozen and stained for senescence-associated beta-galactosidase.

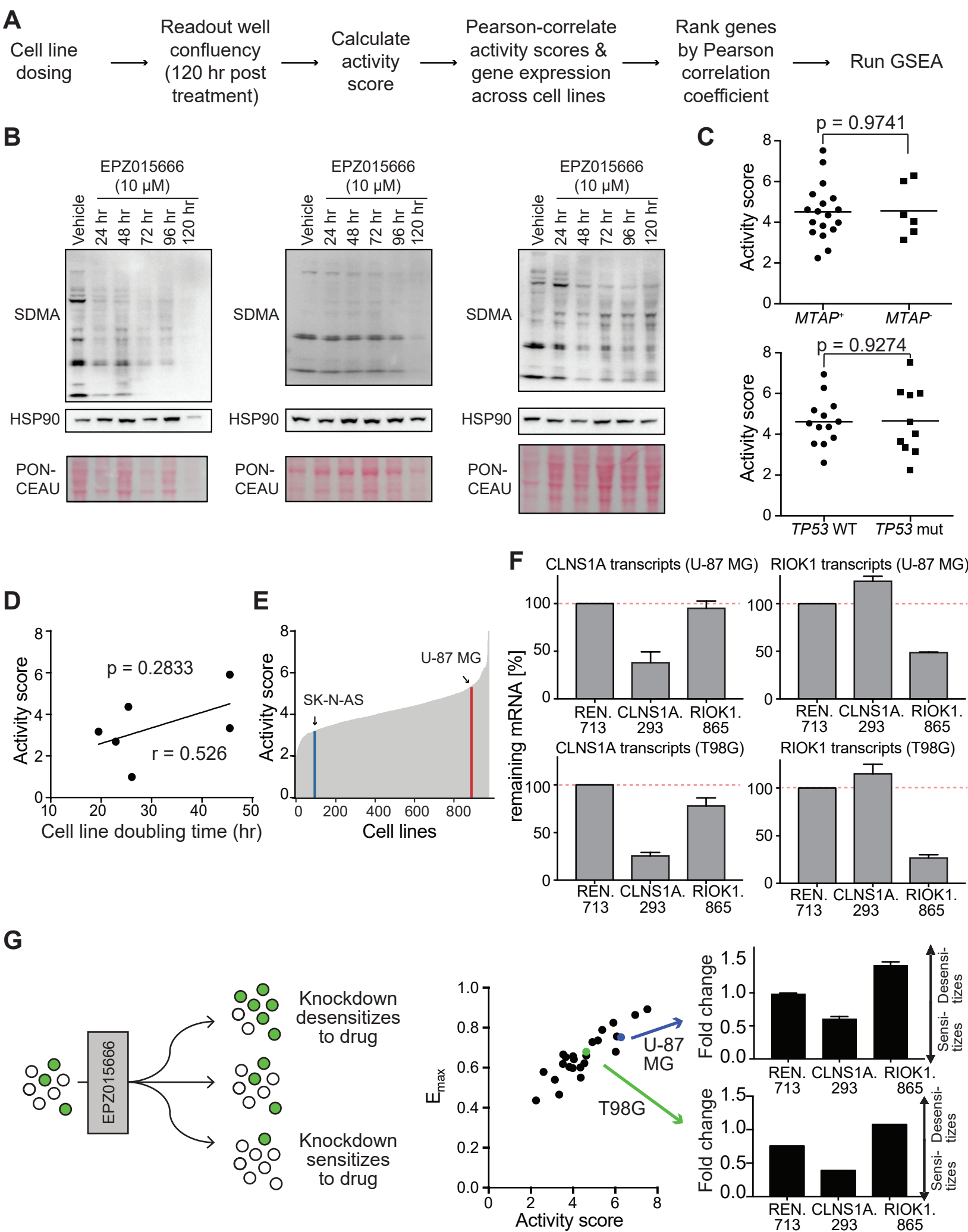
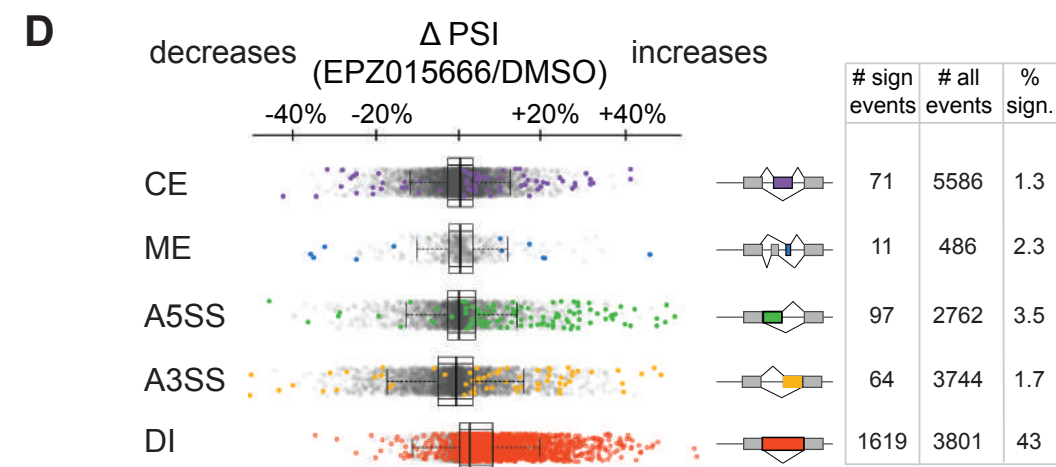
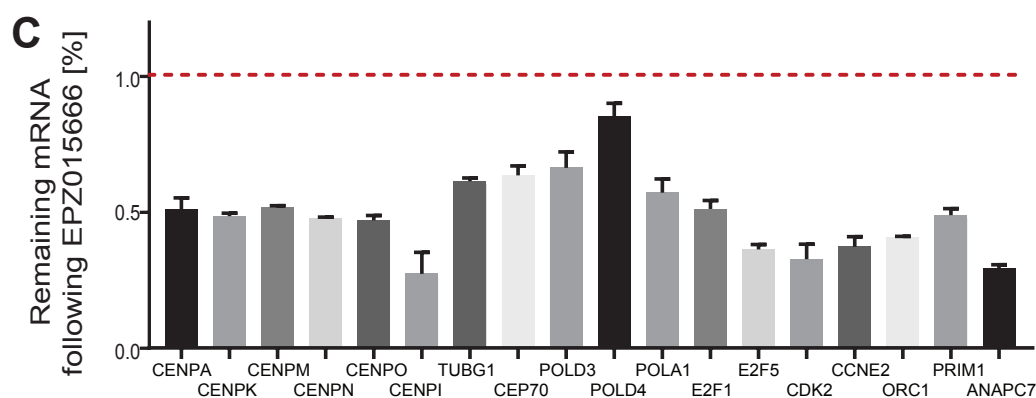
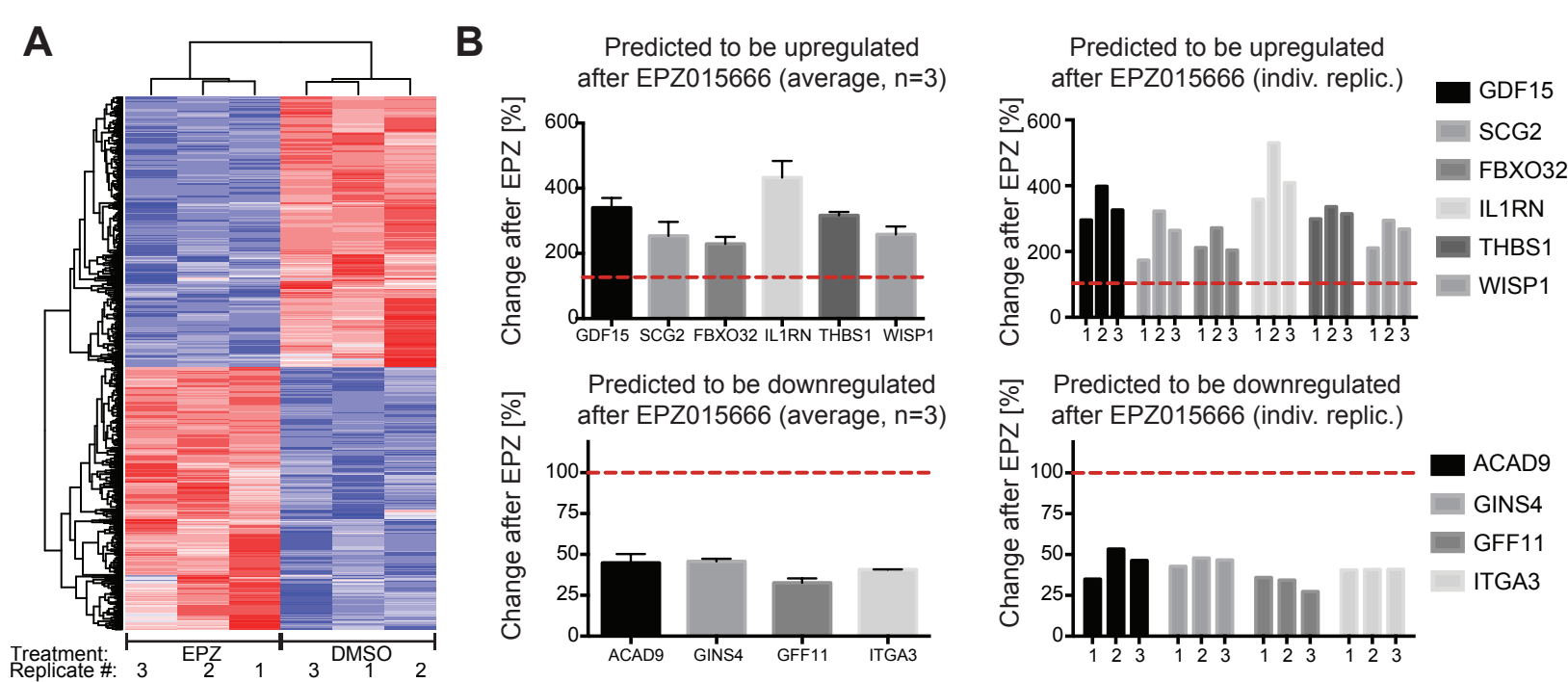


**Figure S5 (related to Figure 5). Whereas *MTAP*- and *TP53*- deletion status does not stratify cell line sensitivities to PRMT5 inhibition, the expression ratio of the two PRMT5 co-factors, CLNS1A and RIOK1, predicts EPZ015666 sensitivity of tumor cells**

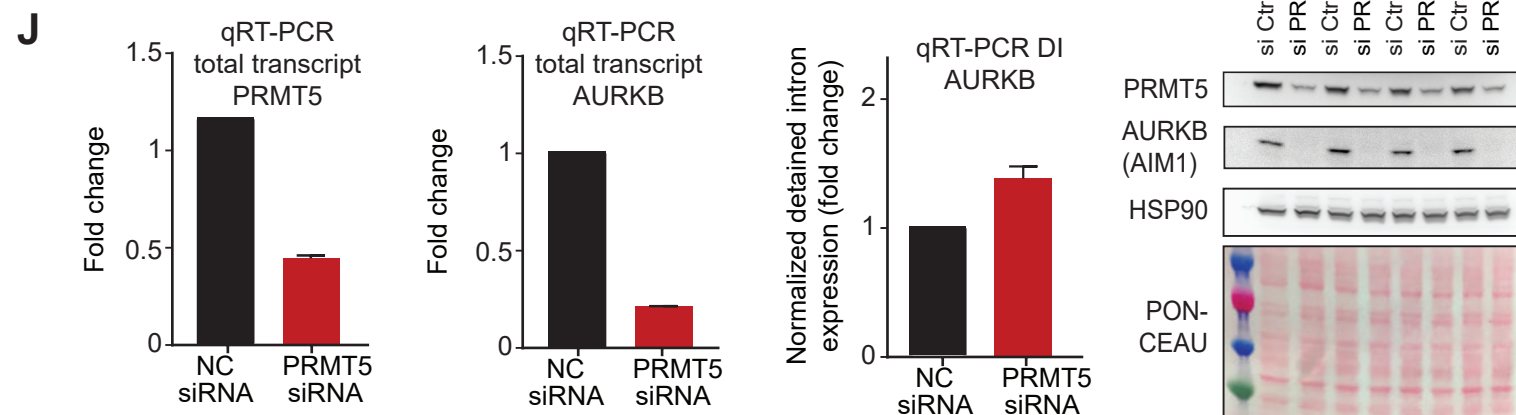
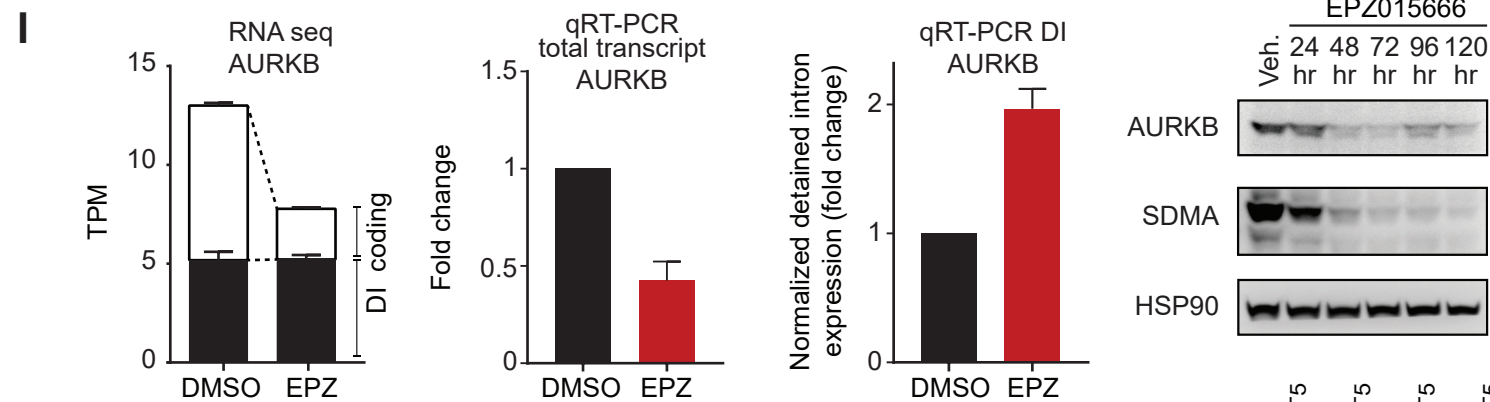
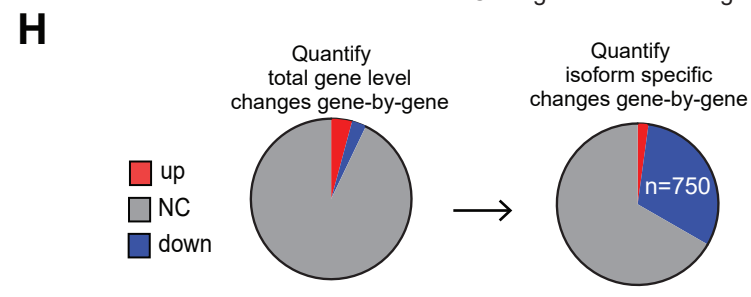
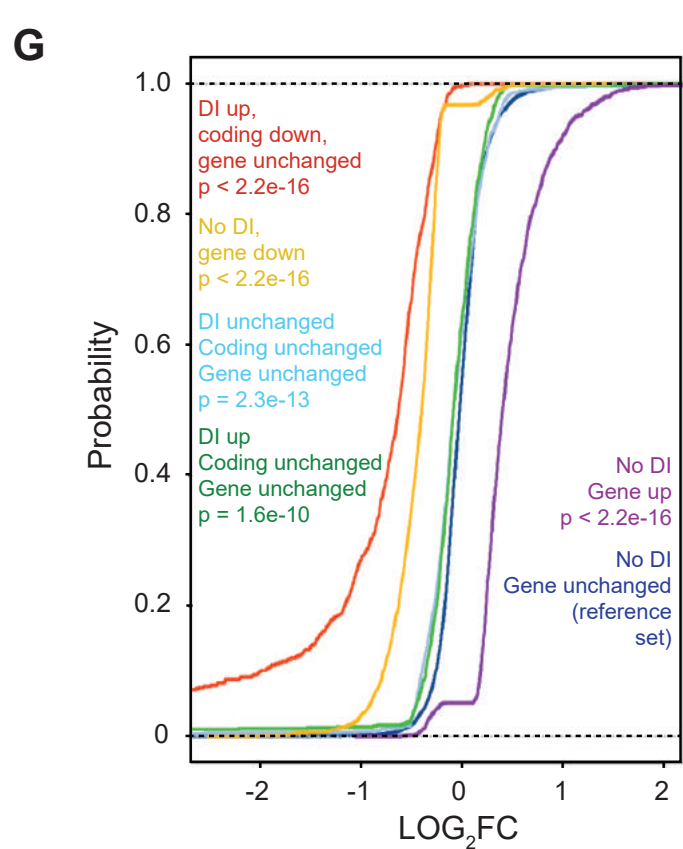
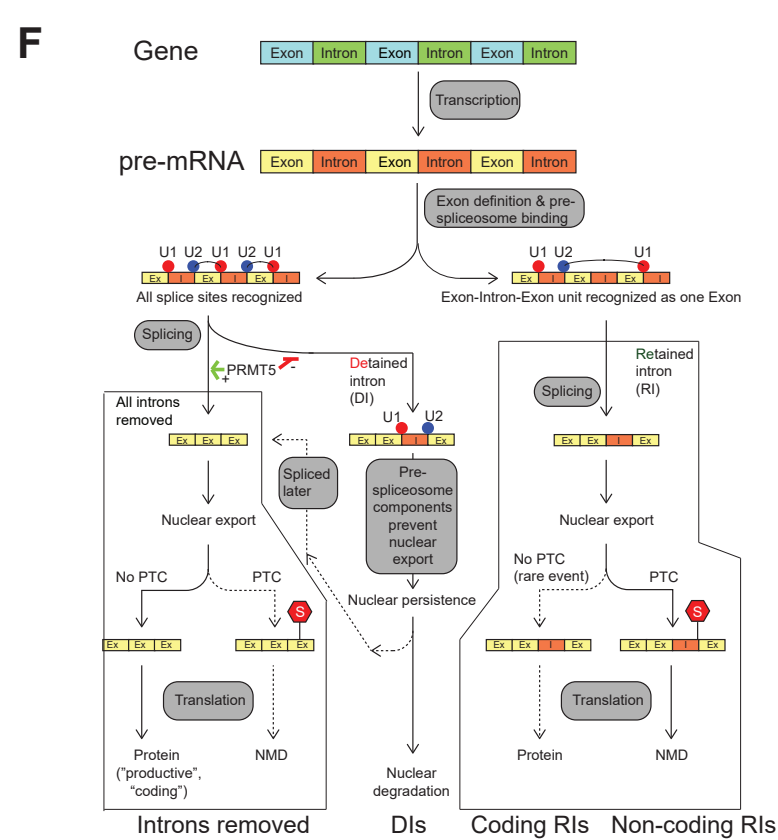
(A) Cell line screen schematic. (B) Immunoblot of SK-N-AS cells (left), SK-MEL-2 cells (middle) and PANC1 cells (right) treated with vehicle or 10  $\mu$ M EPZ015666 over 120 hr. Symmetric dimethyl arginine = SDMA. (C) Activity scores of *MTAP*<sup>+</sup> and *MTAP*<sup>-</sup> cells (top) and activity scores of *TP53* wild-type and *TP53* mutant-cells (bottom). P value represents results of Mann-Whitney test. Horizontal lines represent mean. (D) EPZ015666 activity area and cell line doubling time of n=6 cell lines with linear regression analysis. (E) EPZ015666 activity area for >800 tumor cell lines were predicted based on publicly available CLNS1A and RIOK1 expression levels. (F) Confirmation of shRNA mediated knockdown of endogenous CLNS1A and RIOK1 mRNA by qRT-PCR in U-87 MG and T98G cells. n=3, error bars represent +/- SEM. (G) Starting with a mixed population, cells were treated with EPZ015666 (10  $\mu$ M) for 6 days and analyzed by flow cytometry. Scheme outlining competition assay on the left, results of *in vitro* competition assays in U-87 MG and T98G cells on the right. n=3. Error bars represent +/- SEM.



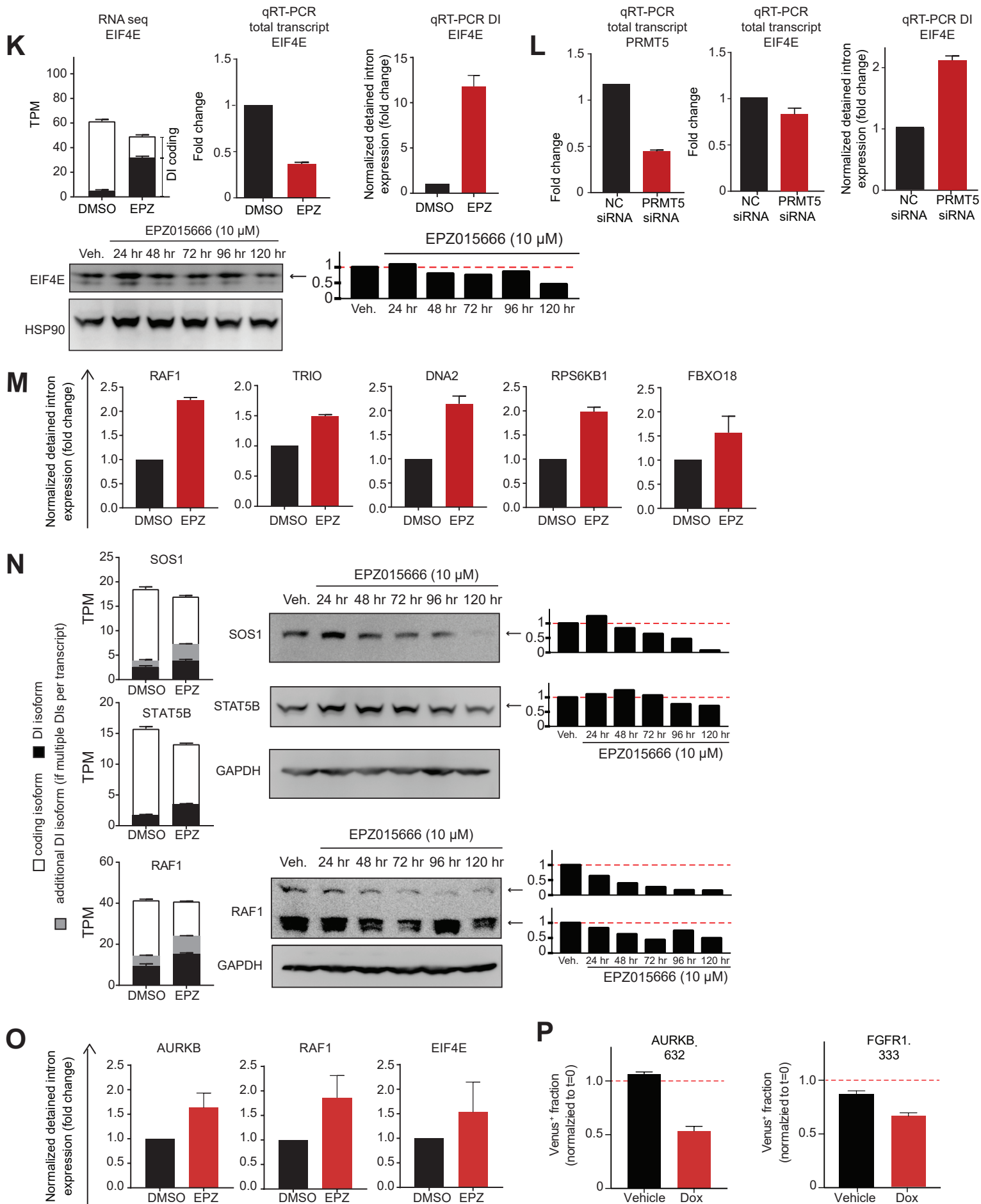
**E**

	Retained Introns (RI)	Detained Introns (DI)
Splice site (SS) regulation	not recognized	recognized
Nuclear export	exported translated	not exported not translated
Nuclear degradation	not degraded	degraded
Translation outcome	Nonsense mediated decay (NMD) or coding sequence	not translated since nuclear detention (if it were exported and translated, it would be NMD substrate)
Bioinformatic distinction	coding RI - in frame coding sequence, no stop codon	internal intron that is predicted NMD substrate but is $\geq 2x$ more abundant than expected, genome wide FDR $< 0.01$

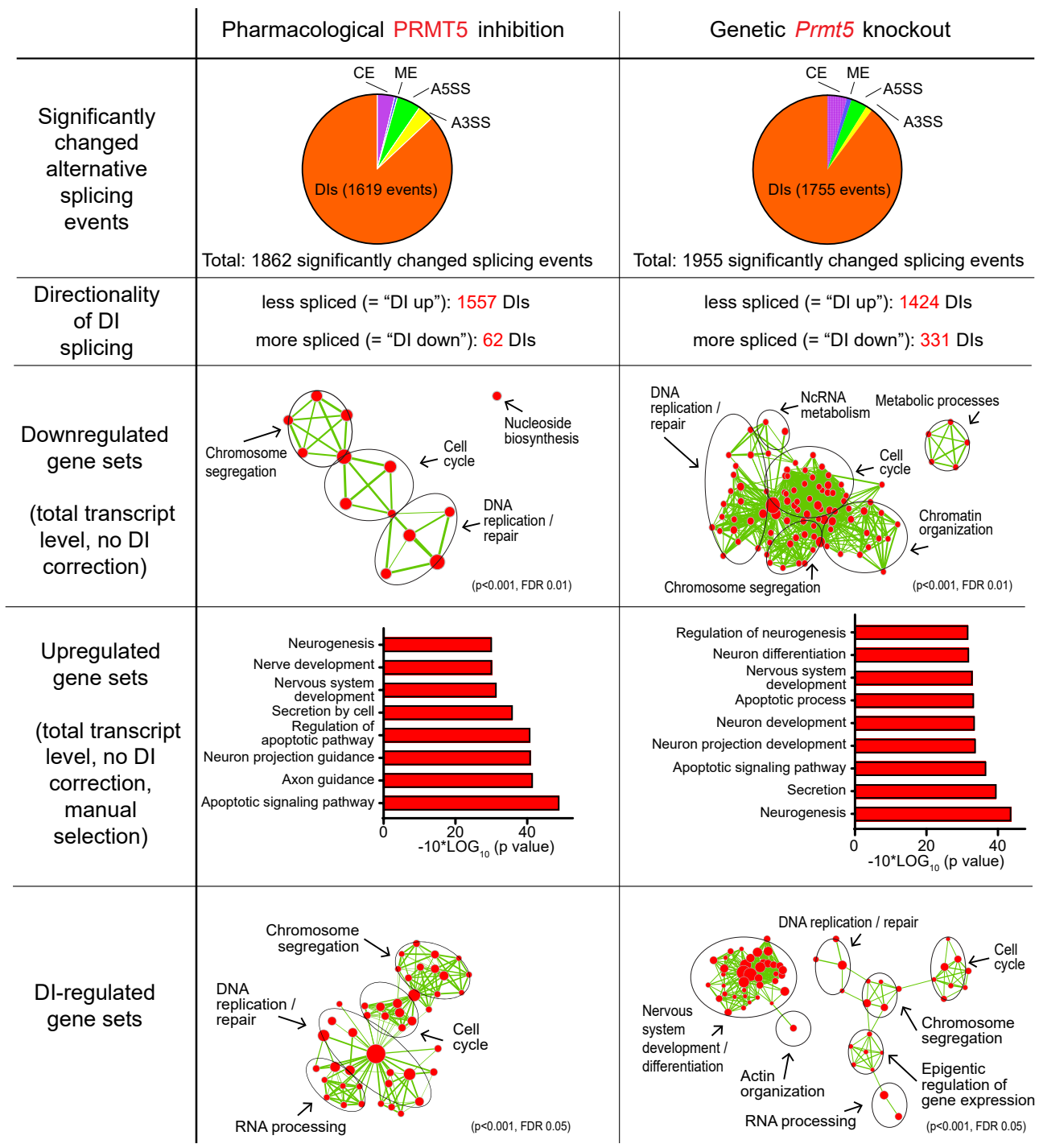




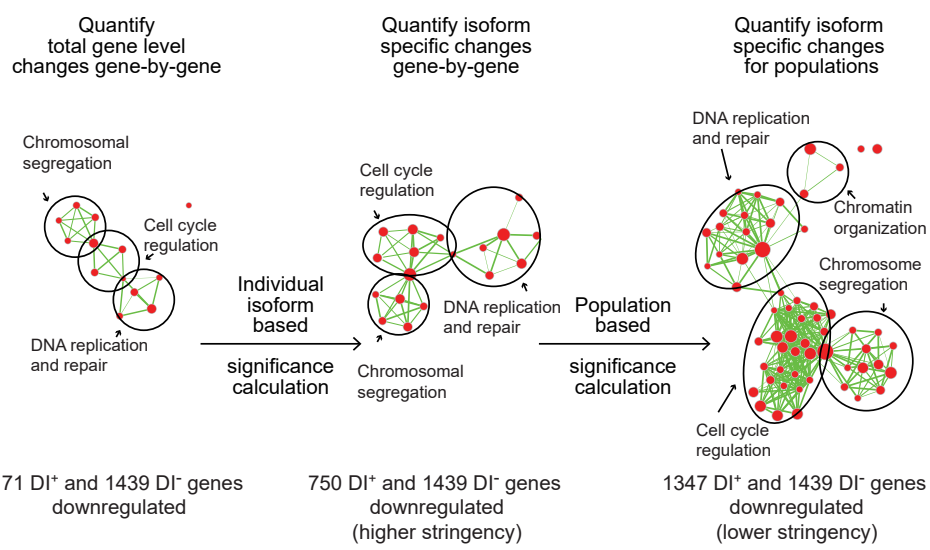




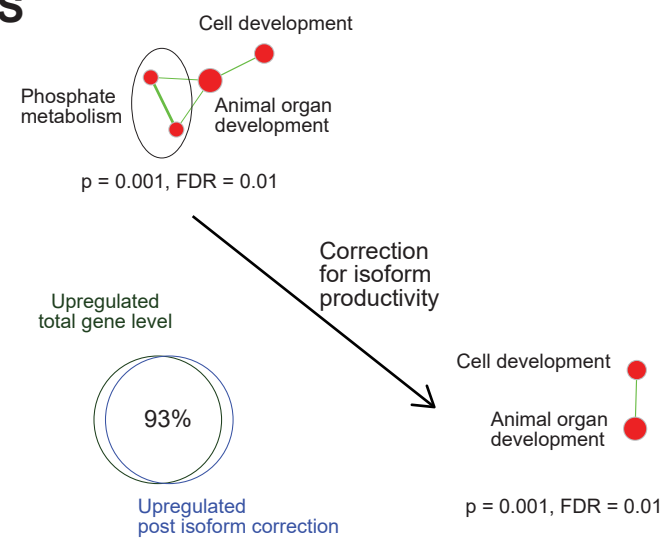
Q



R



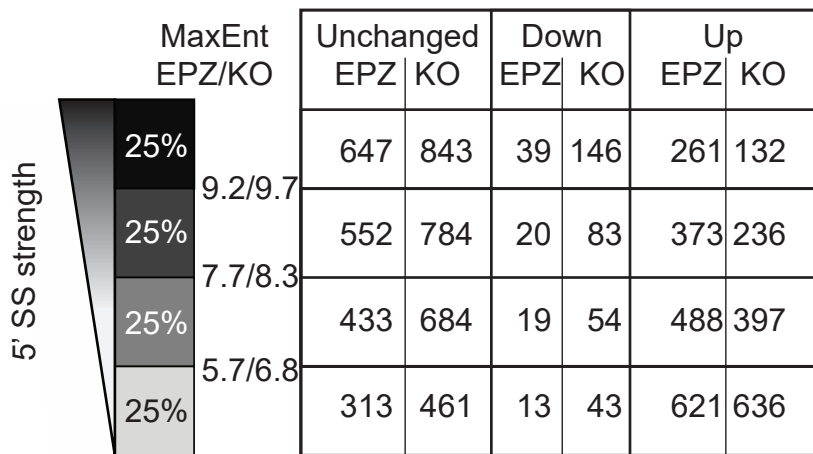
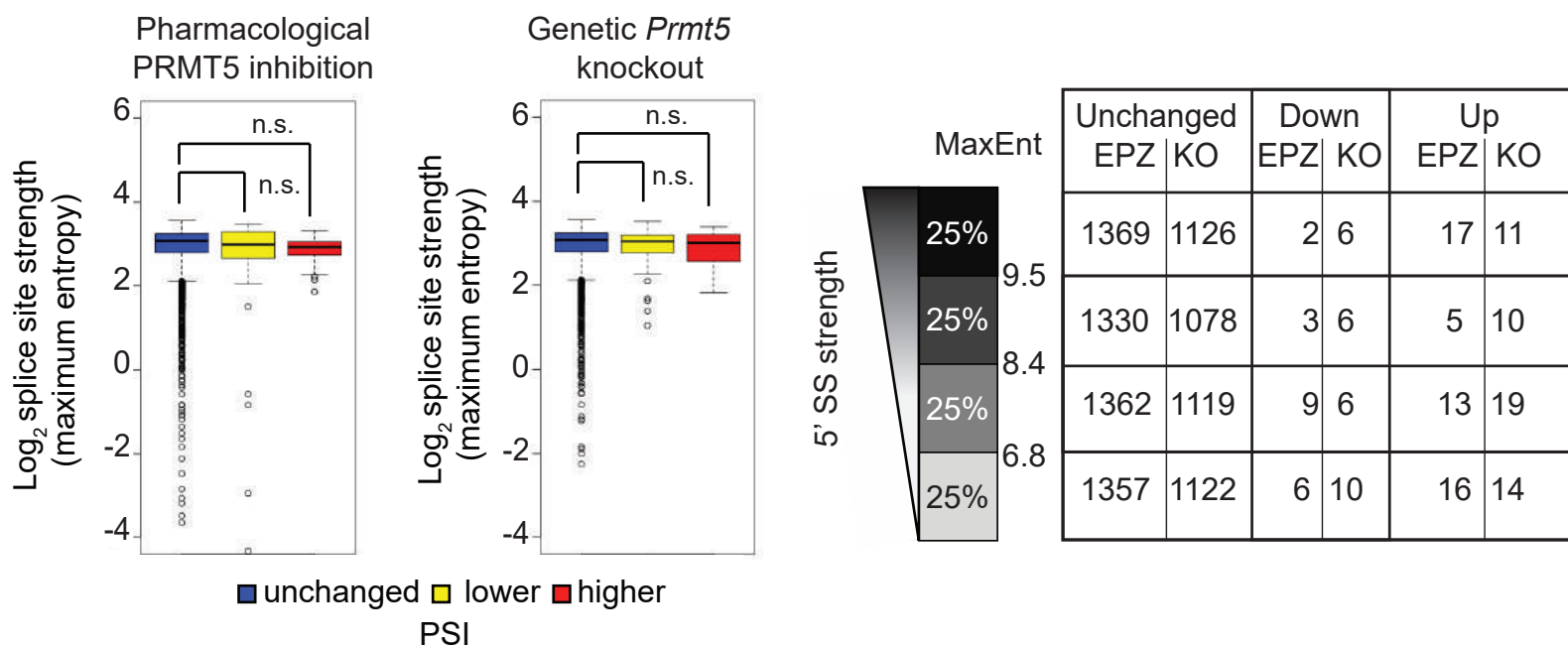
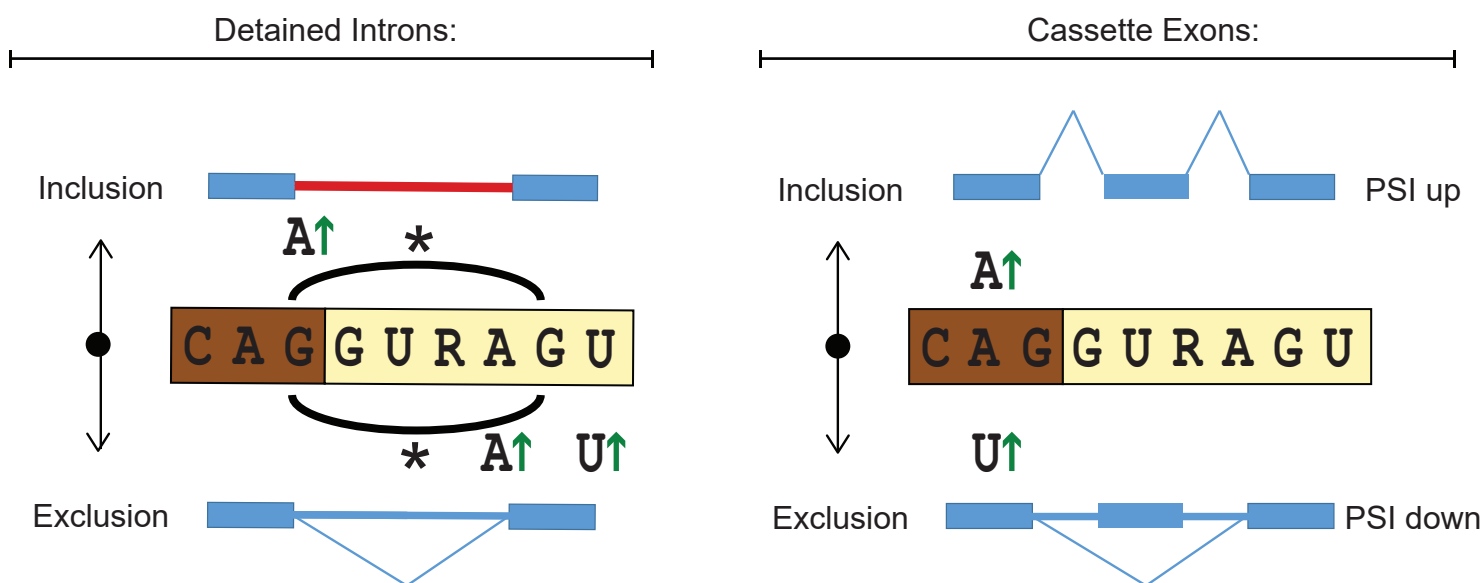
S

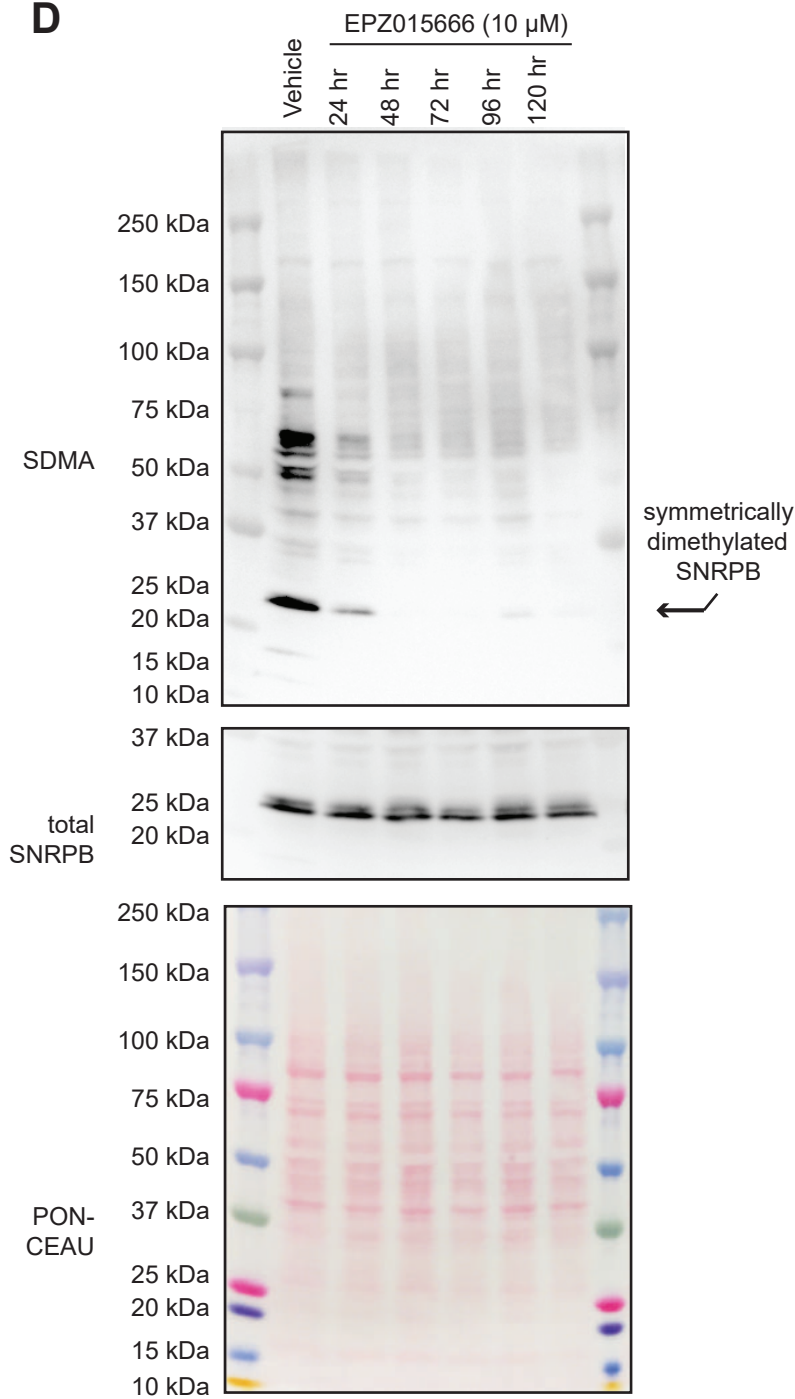
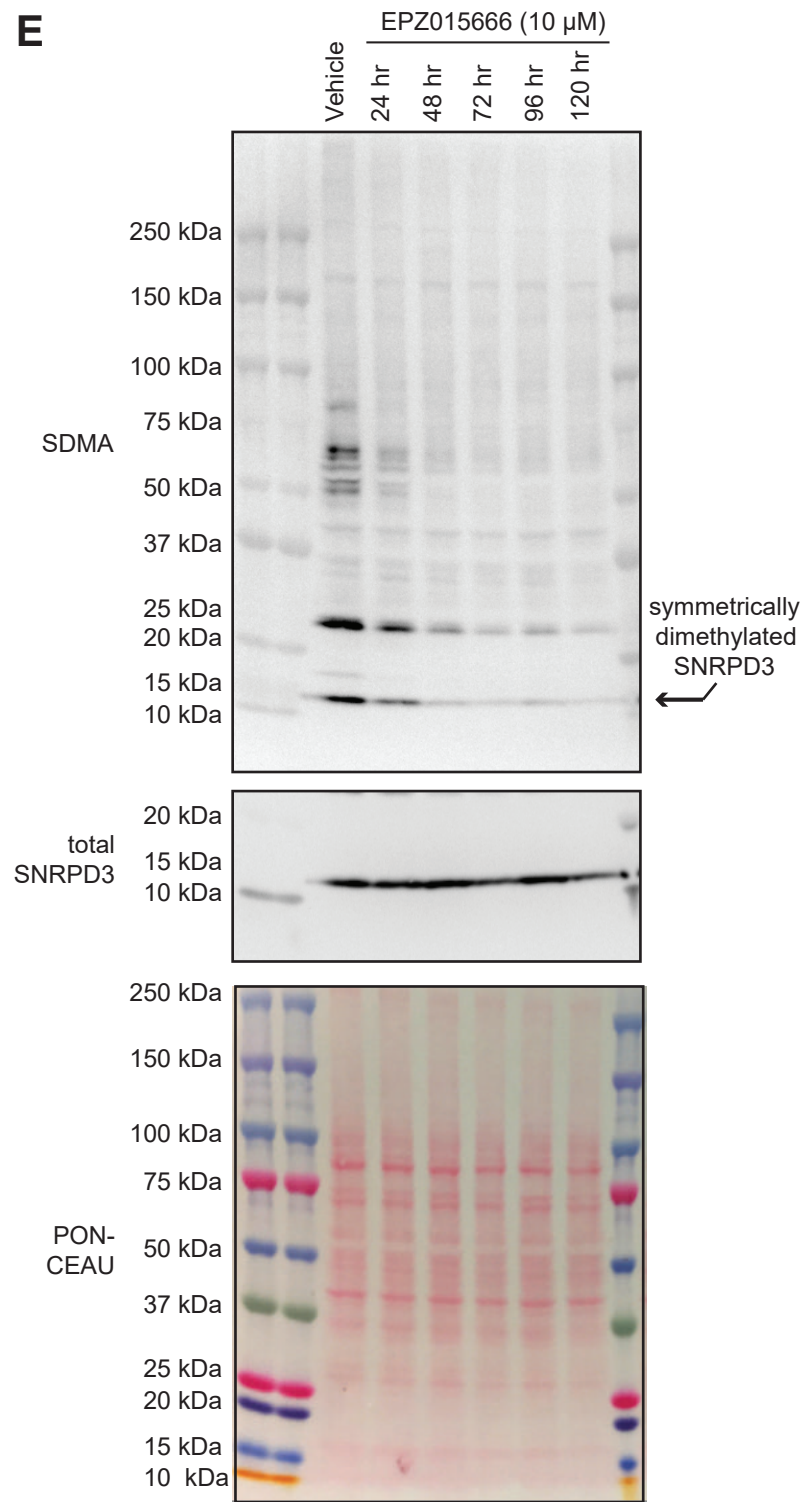
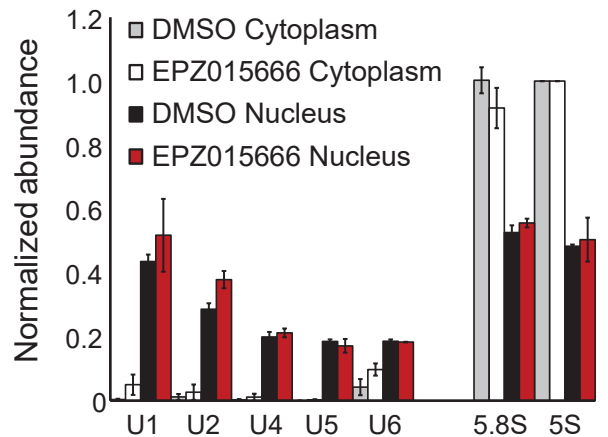
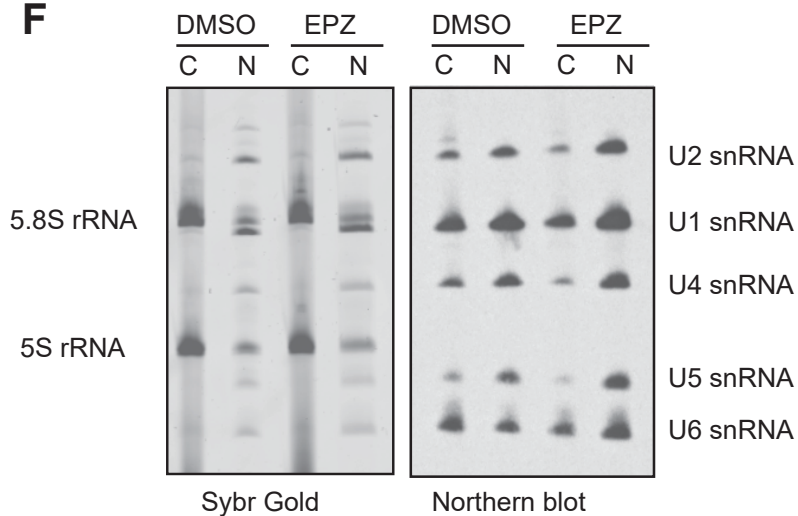


**Figure S6 (related to Figure 6). EPZ015666 treatment causes increase of intron detention and post-transcriptional inactivation of hundreds of proliferation-relevant genes**

(A) Unsupervised clustering of RNAseq samples. 928 genes with PPDE > 0.95 and Log<sub>2</sub>FC >= 0.5. (B) qRT-PCR based validation of RNAseq gene level changes, left graphs show mean and +/- SEM for three replicates, right graphs show individual replicate measurements. (C) qRT-PCR based validation of RNAseq gene level changes with focus on genes involved in cell cycle. n=2, error bars depict +/- SEM. (D) Change in percent spliced in (PSI) of the isoform shown at right between EPZ015666 treatment and control (CE, cassette exon; ME, mutually exclusive exon; A5SS and A3SS, alternative 5' and 3' splice sites, respectively; DI, detained intron). Vertical lines within boxes = median, edges of boxes = 1st and 4th quartiles, whiskers = min/max values, outliers (>/< 1.5 X interquartile range) excluded; table: number of significant events for each AS class, total number of events of each class identified, and the % of the events in each class affected by EPZ015666-treatment. (E) Table contrasting features of both DIs and RIs. (F) Model schematic contrasting detained introns (DIs) and retained introns (RIs). In brief, both DIs and RIs occur within otherwise fully spliced and polyadenylated mRNAs. Whereas DI-containing mRNAs are retained within the nucleus and either degraded there or spliced out later, RI-containing mRNAs are exported to the cytoplasm and either encode alternative peptides or are destroyed by NMD. (G) Cumulative distribution function (CDF) plot showing population-level shifts in expression of the coding isoform of each indicated group of genes as compared to genes with no DI that are unchanged upon EPZ treatment. Significance was determined by two-sided Kolmogorov-Smirnov (KS) tests. (H) Chart extending Fig 6D demonstrating the influence of an isoform-centric analysis for both high-stringency, individual isoform level significance and lower-stringency, population-based statistical analysis for gene expression profiles of 2408 DI<sup>+</sup> genes. (I) Estimation of AURKB gene expression changes in U-87 MG cells following EPZ015666 treatment *in vitro* using different techniques. RNAseq-based estimation of transcripts per million (TPM). Error bars represent +/- SEM (left). qRT-PCR of AURKB total transcript level. Error bars represent +/- SEM, n=2 (second to the left). qRT-PCR of AURKB DI transcripts normalized to total transcript levels, error bars represent +/- SEM, n=2 (third to the left). Immunoblot of AURKB, SDMA and HSP90 protein levels upon EPZ015666 treatment (rightmost). TPM graph is duplication of Fig. 6F, immunoblot is duplication of Fig. 6G. (J) Estimation of AURKB gene expression changes in U-87 MG cells following siRNA mediated knockdown of PRMT5. qRT-PCR of PRMT5 total transcript levels. Error bars represent +/- SEM, n=2 (left). qRT-PCR of AURKB total transcript level. Error bars represent +/- SEM, n=2 (second to the left). qRT-PCR of AURKB DI transcripts normalized to total transcript levels, error bars represent +/- SEM, n=2 (third to the left). Immunoblot of PRMT5, AURKB and HSP90 protein levels upon siRNAs-control or siRNA targeting PRMT5 (rightmost). (K) Estimation of EIF4E gene expression changes in U-87 MG cells following EPZ015666 treatment *in vitro* using different techniques. RNAseq-based estimation of transcripts per million (TPM). Error bars represent +/- SEM (left bar graph). qRT-PCR of EIF4E total transcript levels. Error bars represent +/- SEM, n=2 (middle bar graph). qRT-

PCR of EIF4E DI transcripts normalized to total transcript levels, error bars represent +/- SEM, n=2 (right bar graph). Western blot of EIF4E and HSP90 protein levels upon EPZ015666 treatment with quantification of EIF4E protein levels normalized to HSP90 (bottom). **(L)** Estimation of EIF4E gene expression changes in U-87 MG cells following siRNA mediated knockdown of PRMT5. qRT-PCR of PRMT5 total transcript levels, n=2. Error bars represent +/- SEM (left, duplication of graph depicted in (Fig S6J)). qRT-PCR of EIF4E total transcript levels. Error bars represent +/- SEM, n=2 (middle). qRT-PCR of EIF4E DI transcripts normalized to total transcript levels, error bars represent +/- SEM, n=2 (right). **(M)** qRT-PCR of DI transcripts of different genes normalized to the corresponding total transcript levels following EPZ015666 treatment, error bars represent +/- SEM, n=2. **(N)** Transcript per million (TPM) plots and immunoblots of U-87 MG cells treated with 10  $\mu$ M EPZ015666 for the indicated time points and quantification. In TPM-plots, white bar indicates coding isoform, black bar indicates isoform with one detained intron, grey bar indicates isoform with a different detained intron for genes with multiple detained introns. Error bars represent +/- SEM. Quantifications of the immunoblots normalized to control gene expressions are shown at right. **(O)** qRT-PCR of DI transcripts of different genes normalized to the corresponding total transcript levels in PDX *in vivo* tumors. Error bars represent +/- SEM. Mice had been treated with vehicle (n=2) or EPZ015666 (n=2) starting 9 days post tumor injection. Mice were euthanized upon morbidity (roughly three weeks post tumor injection). **(P)** *In vitro* competition assays of U-87 MG following knockdown of AURKB and FGFR1 (as estimated by flow cytometry 7 days following Dox-based shRNA induction, n=3, error bars represent +/- SEM). **(Q)** Detailed comparison of gene expression and splicing changes following either EPZ015666 treatment of U-87 MG cells for 72 hr (left column) or the genetic knockout of *Prmt5* in murine neuro-progenitor / stem cells (right column). Network maps display enriched gene sets in all genes down-regulated by PRMT5 inhibition / knockout versus all expressed genes (third row) and in DI-containing genes versus all expressed genes (fifth row). Each node represents a significantly enriched gene set, the size of which is proportional to the gene number and the width of the green edges indicating the degree of gene overlap between nodes. Clusters of functionally related gene sets are circled and labeled. **(R)** Network maps display enriched gene set in genes down-regulated post EPZ015666 treatment of U-87 MG cells versus all expressed in the absence of isoform correction (depicted left), following gene-by-gene isoform correction (more stringent, depicted in the middle) and following population based isoform correction (less stringent, depicted right), including both DI and non-DI containing genes. **(S)** Network maps display enriched gene set in genes up-regulated post EPZ015666 treatment of U-87 MG cells versus all expressed in the absence of isoform correction (left map) and following gene-by-gene isoform correction (right map), including both DI and non-DI containing genes. Venn diagram displays percentage of genes classified as up-regulated post EPZ015666 treatment in the absence of isoform correction (left circle) and following isoform correction (right circle).

**A****B****C**

**D****E****F**



**Figure S7 (related to Figure 7). 5' splice site strength is not the sole determinant of PRMT5-dependent splicing changes. SnRNPs lose symmetric arginine dimethylation marks upon PRMT5 inhibition but exhibit no gross changes in stability or subcellular localization.**

(A) The number of DIs falling within each quartile of relative 5' splice site strengths of all DIs are shown for the sets of DIs that are unchanged, downregulated or upregulated following EPZ015666 treatment of U-87 MG cells or *Prmt5* knockout in NPCs. 5' splice site strength scores were determined by MaxEnt; cutoff scores defining each quartile are shown for the EPZ015666 and *Prmt5* knockout sets. (B) Relative strengths of 5' and 3' splice sites of CEs (determined by MaxEnt) that are not significantly changed (blue), down-regulated (yellow), or up-regulated (red) by PRMT5 inactivation for both pharmacological PRMT5 inhibition in U-87 MG cells by EPZ015666 (left boxplot) and genetic knockout of *Prmt5* in NPCs (right boxplot). The number of cassette exons falling within each quartile of relative 5' splice site strengths of all cassette exons are shown for the sets of exons that are unchanged, down-regulated or up-regulated following EPZ015666 treatment of U-87 MG cells or *Prmt5* knockout in NPCs. 5' splice site strength scores were determined by MaxEnt; cutoff scores defining each quartile are shown and were identical between the EPZ015666 and *Prmt5* knockout sets. Horizontal lines within boxes = median, edges of boxes = 1st and 4th quartiles, whiskers = min/max values, outliers excluded; points = outliers  $>/< 1.5 \times$  interquartile range (C) Schematic drawing illustrating the correlative impact of base exchanges in the 5' splice site on inclusion of either DIs (left) or CEs (right). Single bases below or above the consensus sequence indicate individual bases that are either correlated with increased inclusion (above the consensus splice site sequence) or exclusion (below consensus splice site sequence). \* = For DIs, the presence of Gs in both positions -1 and +5 is highly correlated with DI exclusion, whereas the presence of a nucleotide other than G in either -1 or +5, or both, is highly correlated with DI inclusion. (D) Immunoblot of U-87 MG cells treated with EPZ015666 or vehicle for the indicated time points. Due to the lack of commercial availability of an antibody specifically binding dimethylated SNRPB, we visualized total SDMA, stripped the membrane and visualized total SNRPB allowing for size estimation. (E) Immunoblot of U-87 MG cells treated with EPZ015666 or vehicle for the indicated time points. Due to the lack of commercial availability of an antibody specifically binding dimethylated SNRPD3, we visualized total SDMA, stripped the membrane and visualized total SNRPD3 allowing for size estimation. (F) U-87 MG cells were treated with either EPZ015666 or vehicle for 72 hr followed by the separate extraction of nuclear and cytoplasmic RNA fractions. RNA from equal cell numbers was then separated by Polyacrylamide gel electrophoresis and either visualized by Sybr gold staining or transferred on a membrane for specific visualization of indicated snRNAs by northern blot. Abundance of RNA species was estimated and normalized to 5S rRNA / DMSO control across three replicates. Error bars represent  $\pm$  SEM.

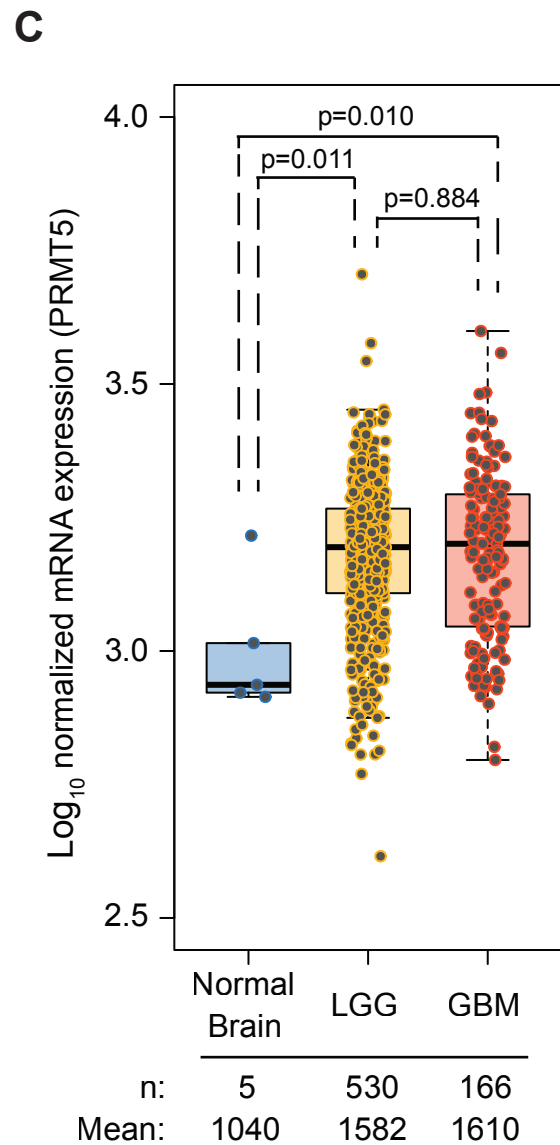
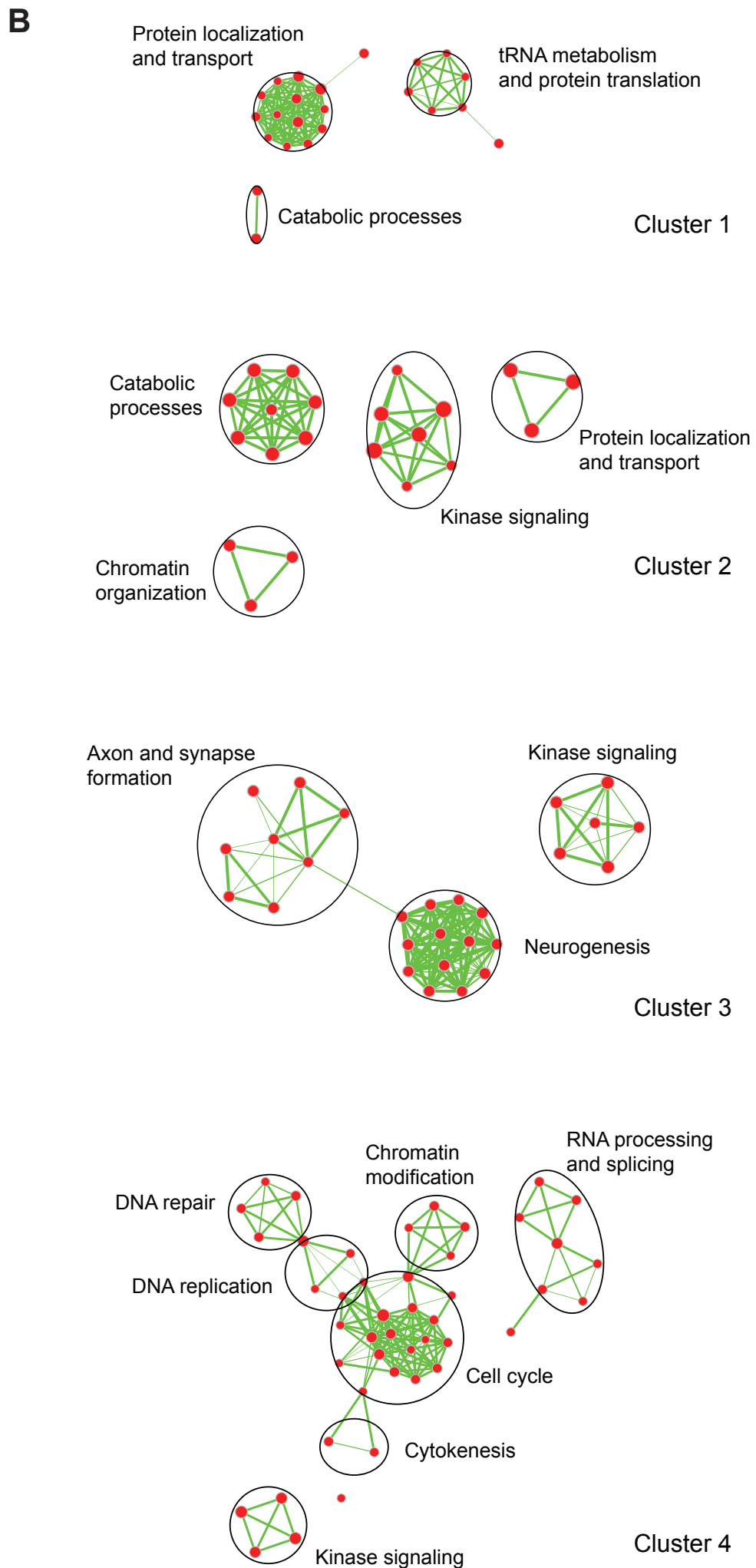
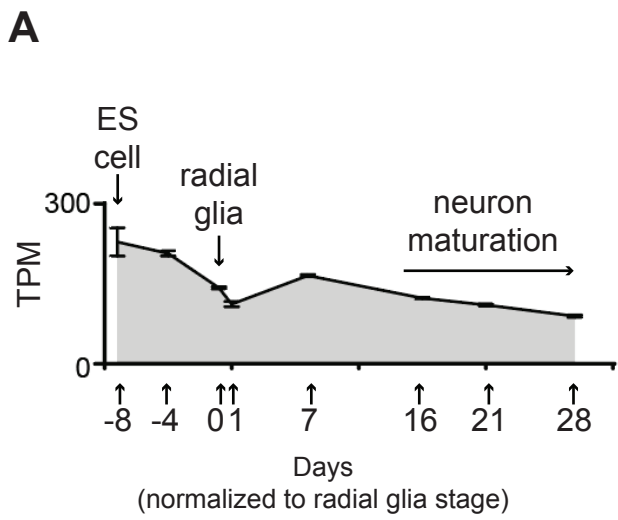


**Figure S8 (related to Figure 8). Coordination of detained intron splicing contributes to gene expression regulation upon neural differentiation**

(A) PRMT5 Transcripts Per Kilobase Million (TPM) levels at different time points upon differentiation of ES cells into neurons. (B) Network maps display significantly enriched gene sets within the indicated neuro-differentiation gene cluster versus all expressed genes with functionally related gene sets circled and labeled. (C) PRMT5 mRNA expression levels in patients (LGG=Low grade glioma, GBM = glioblastoma multiforme). The Wilcoxon Rank-Sum test was employed to estimate significance. Horizontal lines within boxes = median, edges of boxes = 1st and 4th quartiles, whiskers = min/max values, outliers excluded; points = outliers  $>/< 1.5 \times$  interquartile range.